

DARK MATTER DEFICIENT GALAXIES IN THE ILLUSTRIS FLAT- Λ CDM MODEL STRUCTURE FORMATION SIMULATION

HAI YU,^{1,2,*} BHARAT RATRA,^{2,†} AND FA-YIN WANG^{1,3,‡}

¹*School of Astronomy and Space Science, Nanjing University, Nanjing 210093, China*

²*Department of Physics, Kansas State University, 116 Cardwell Hall, Manhattan, KS 66506, USA*

³*Key Laboratory of Modern Astronomy and Astrophysics (Nanjing University), Ministry of Education, Nanjing 210093, China*

(Dated: September 18, 2018)

ABSTRACT

Surveying dark matter deficient galaxies (those with dark matter mass to stellar mass ratio $M_{\text{dm}}/M_{\text{star}} < 1$) in the Illustris simulation of structure formation in the flat- Λ CDM cosmogony, we find $M_{\text{star}} \approx 2 \times 10^8 M_{\odot}$ galaxies that have properties similar to those ascribed by van Dokkum et al. (2018a) to the ultra-diffuse galaxy NGC1052-DF2. The Illustris simulation also contains more luminous dark matter deficient galaxies. Illustris galaxy subhalo 476171 is a particularly interesting outlier, a massive and very compact galaxy with $M_{\text{star}} \approx 9 \times 10^{10} M_{\odot}$ and $M_{\text{dm}}/M_{\text{star}} \approx 0.1$ and a half-stellar-mass radius of ≈ 2 kpc. If the Illustris simulation and the Λ CDM model are accurate, there are a significant number of dark matter deficient galaxies, including massive luminous compact ones. It will be interesting to observationally discover these galaxies, and to also more clearly understand how they formed, as they are likely to provide new insight into and constraints on models of structure formation and the nature of dark matter.

Keywords: galaxies: kinematics and dynamics — galaxies: structure — galaxies: formation — galaxies: evolution — galaxies: individual: NGC1052-DF2 — dark matter

* yuhai@smail.nju.edu.cn

† ratra@phys.ksu.edu

‡ fayinwang@nju.edu.cn

1. INTRODUCTION

In the standard Λ CDM model (Peebles 1984) the cosmological constant Λ powers the currently accelerating cosmological expansion and cold dark matter (CDM) is now the second biggest contributor to the cosmological energy budget. Earlier, when nonrelativistic CDM and baryonic matter dominated, the cosmological expansion decelerated. The standard spatially-flat Λ CDM model is consistent with many observational constraints when the current Λ , CDM, and baryonic density parameters are at or near $\Omega_\Lambda = 0.70$, $\Omega_c = 0.25$, and $\Omega_b = 0.05$ (Park & Ratra 2018b).¹

These observations include cosmic microwave background (CMB) anisotropies (Hinshaw et al. 2013; Planck Collaboration 2016), baryon acoustic oscillation distances (Alam et al. 2017; Ryan et al. 2018), supernova Type Ia apparent magnitudes (Scolnic et al. 2017), and Hubble parameters (Farooq et al. 2017; Yu et al. 2018). There is significant observational evidence for CDM, as well as for Λ (or a dark energy that behaves almost like Λ), and introducing these fairly astonishing hypothetical substances appears to be the most reasonable way to make sense of the observations. For instance, Hubble parameter observations span a wide redshift range, almost to $z = 2.4$, and show evidence for both a present epoch dark energy powered accelerating cosmological expansion as well as an earlier CDM and baryonic matter driven decelerated cosmological expansion (Farooq & Ratra 2013; Farooq et al. 2013; Moresco et al. 2016; Farooq et al. 2017; Yu et al. 2018; Jesus et al. 2018; Haridasu et al. 2018). It is also widely accepted that CDM is necessary for the formation of observed structure in the cosmological matter and radiation fields.

In the standard CDM structure formation model (Peebles 1982), quantum zero-point fluctuations of the inflaton scalar field during inflation (Hawking 1982; Starobinsky 1982; Guth & Pi 1982; Fischler et al. 1985) seeded spatial inhomogeneities that then grew under gravitational instability to create the observed structures in the cosmological matter and radiation fields. Initially inhomogeneities developed and grew in the CDM; as the CMB cooled and decoupled from the baryons, baryonic matter was gravitationally attracted to and fell deeper into the CDM halo inhomogeneity gravitational potential wells. While the initial gathering of CDM under gravity is a relatively simple process, when the baryons start to play a significant role the structure formation problem becomes much less tractable because the physics is more familiar, more complex, and more difficult to model quantitatively.

In the standard Λ CDM model it is not inconceivable that after a collection of baryonic matter formed stars and became a “galaxy”, this galaxy might be ejected from the CDM halo in which it was formed and could find itself in a region with a lower CDM density.² It is not known how probable such an outcome is. The van Dokkum et al. (2018a) observations and argument that the ultra-diffuse dwarf galaxy NGC1052-DF2 has a stellar mass of about $2 \times 10^8 M_\odot$ and a total mass of less than $3.4 \times 10^8 M_\odot$ in a radius of 7.6 kpc and so indicates a much smaller dark matter mass to stellar mass ratio, $M_{\text{dm}}/M_{\text{star}}$, than that of a typical galaxy with this stellar mass,³ motivated us to attempt to determine the probability of such an outcome.

We study the issue of dark matter deficient galaxies by looking at galaxy population statistics of the Illustris simulation (www.illustris-project.org, Vogelsberger et al. 2014a) of structure formation in the flat- Λ CDM cosmogony. We find that dark matter deficient galaxies, with $M_{\text{star}} \approx 2 \times 10^8 M_\odot$ and $M_{\text{dm}}/M_{\text{star}} < 1$ (like NGC1052-DF2, van Dokkum et al. 2018a), are not uncommon. We also find a significant number of more luminous and more massive dark matter deficient galaxies.

2. DARK MATTER DEFICIENT GALAXY STATISTICS AND EXAMPLES

Illustris (www.illustris-project.org, Vogelsberger et al. 2013, 2014a,b; Genel et al. 2014; Sijacki et al. 2015) is one of the largest hydrodynamical cosmological simulations. It can help us understand how structure in the universe evolves with time, and in particular how the dark matter and stellar mass distributions evolve. The simulation assumes a tilted spatially-flat Λ CDM cosmogony with chosen parameter values in reasonable accord with current cosmological measurements (Park & Ratra 2018b).⁴ The fiducial parameter values chosen for the simulation are $(\Omega_m, \Omega_\Lambda, \Omega_b, \sigma_8, n_s, h) = (0.2726, 0.7274, 0.0456, 0.809, 0.963, 0.704)$ coming from the final WMAP analysis (Hinshaw et al. 2013).⁵ The Illustris-1 simulation contains 1820^3 dark matter particles, 1820^3 gas particles, and 1820^3 tracer

¹ For reviews of the standard model see Ratra & Vogeley (2008), Martin (2012), and Luković et al. (2018).

² It is highly unlikely that baryonic structure, a “galaxy”, could form in very low CDM density regions.

³ We note that there has been some discussion of these observations and the van Dokkum et al. (2018a) interpretation of them (van Dokkum et al. 2018b; Martin et al. 2018; Laporte et al. 2018; Famaey et al. 2018; Scarpa et al. 2018; Nusser 2018; Trujillo et al. 2018; van Dokkum et al. 2018c; Wasserman et al. 2018; Blakeslee & Cantiello 2018).

⁴ Current cosmological data are also not inconsistent with mildly closed spatial hypersurfaces (Ooba et al. 2018a; Park & Ratra 2018a,b,d), with mild dark energy dynamics (Ooba et al. 2018c; Park & Ratra 2018b,c,d), and with nonflat dynamical dark energy models (Ooba et al. 2017, 2018b; Park & Ratra 2018b,c,d). While reionization is remarkably different in the closed model compared to the standard flat case (Mitra et al. 2018), it is likely that structure formation will be less affected by observationally-consistent values of nonzero spatial curvature or dark energy dynamics.

⁵ Here Ω_m is the nonrelativistic matter density parameter, σ_8 is the rms fractional energy density inhomogeneity averaged over $8h^{-1}$ Mpc spheres, n_s is the spectral index of the primordial energy density perturbation power spectrum (which is assumed to be a power law in wavenumber), and h is the Hubble constant in units of $100 \text{ km s}^{-1} \text{ Mpc}^{-1}$.

| SUBFIND ID | M_{tot} ($10^{10} M_{\odot}$) | M_{dm} ($10^{10} M_{\odot}$) | M_{star} ($10^{10} M_{\odot}$) | M_{gas} ($10^{10} M_{\odot}$) | SFR (M_{\odot}/yr) | $r_{1/2}$ (kpc) | r_{ph} (kpc) |
|---------------|---|--|--|---|----------------------------------|--------------------|--------------------------|
| 41124 | 4.45 | 0.260 | 4.18 | 0 | 0 | 2.03 | 5.24 |
| 231881 | 1.86 | 0.0726 | 1.79 | 0 | 0 | 1.57 | 2.49 |
| 476171 | 10.54 | 0.915 | 9.42 | 0 | 0 | 1.82 | 4.76 |
| 41089 | 2645.03 | 2587.20 | 52.94 | 4.67 | 0.0036 | 28.68 | 19.27 |
| 231879 | 1752.37 | 1692.51 | 57.81 | 1.85 | 0 | 17.47 | 21.83 |
| 928035 | 0.0659 | 0 | 0.0659 | 0 | 0 | 1.75 | 1.32 |

Table 1. First three data rows list the properties of the three massive dark matter deficient subhalos in snap 135 at $z = 0$. Fourth and fifth data rows give properties of the subhalos that subhalos 41124 and 231881 are merging with. Last data row lists properties of subhalo 928035 which is discussed below. M_{tot} , M_{dm} , M_{star} and M_{gas} are total mass, dark matter mass, stellar mass, and gas mass of the subhalos. SFR is the star formation rate, $r_{1/2}$ is the half-stellar-mass radius (the radius containing half of the stellar mass of this subhalo), and r_{ph} is the stellar photometric radius (the radius at which the surface brightness profile, computed from all member stellar particles, drops below the limit of 20.7 mag arcsec $^{-2}$ in the K band).



Figure 1. The mock images of the three massive dark matter deficient subhalos. From left to right, these are for 41124, 231881, and 476171 respectively.

particles in a comoving box of size $(106.5 \text{ Mpc})^3$. The mass of each dark matter particle is $6.26 \times 10^6 M_{\odot}$ and for baryonic particles the mass is $1.26 \times 10^6 M_{\odot}$. The simulation not only accounts for gravity and hydrodynamics but also includes effects of star formation and evolution, gas cooling, black holes and supermassive black hole feedback, as well as other relevant phenomena, and so should allow us to have a fuller understanding of the effects of various physical processes on the formation of large-scale structure. In this work we make use of the Illustris-1 simulation.

At redshift $z = 0$ there are 7,713,601 friends-of-friends (FoF) groups (with more than 32 dark matter particles) and 4,366,546 individual SUBFIND (gravitationally bound) subhalos have formed (Vogelsberger et al. 2014a,b). The present time, at $z = 0$, corresponds to snapshot or snap 135.⁶ We use the subhalo catalog to get the dark matter mass, M_{dm} , and the stellar mass, M_{star} , of each SUBFIND subhalo and find that most of them have zero stellar mass.⁷ Ignoring these leaves 307,786 subhalos, about 7.0% of all subhalos. We then select subhalos with $M_{\text{dm}} < M_{\text{star}}$, finding 4216 subhalos which have more stellar mass than dark matter mass, about 1.3% of the subhalos that have nonzero stellar mass. Most of these have low stellar mass, less than $10^{10} M_{\odot}$. There are however three subhalos with stellar mass greater than $10^{10} M_{\odot}$ with $M_{\text{dm}}/M_{\text{star}} < 0.1$.

The SUBFIND IDs of these three massive dark matter deficient subhalos are 41124, 231881 and 476171 in snap 135 at $z = 0$ and their properties are listed in Table 1. We see that these subhalos have no gas and their star formation has

⁶ 136 data snapshots are stored for each Illustris run, the first one, snap 0, is at $z = 46.773$.

⁷ These subhalo masses are Illustris SubhaloMassType masses. These are the total masses of all member particle/cells which are bound to the subhalo under consideration, separated by type. SubhaloMassType does not account for particle/cells bound to substructures of the subhalo under consideration. Later in this paper we will also use two other mass definitions.

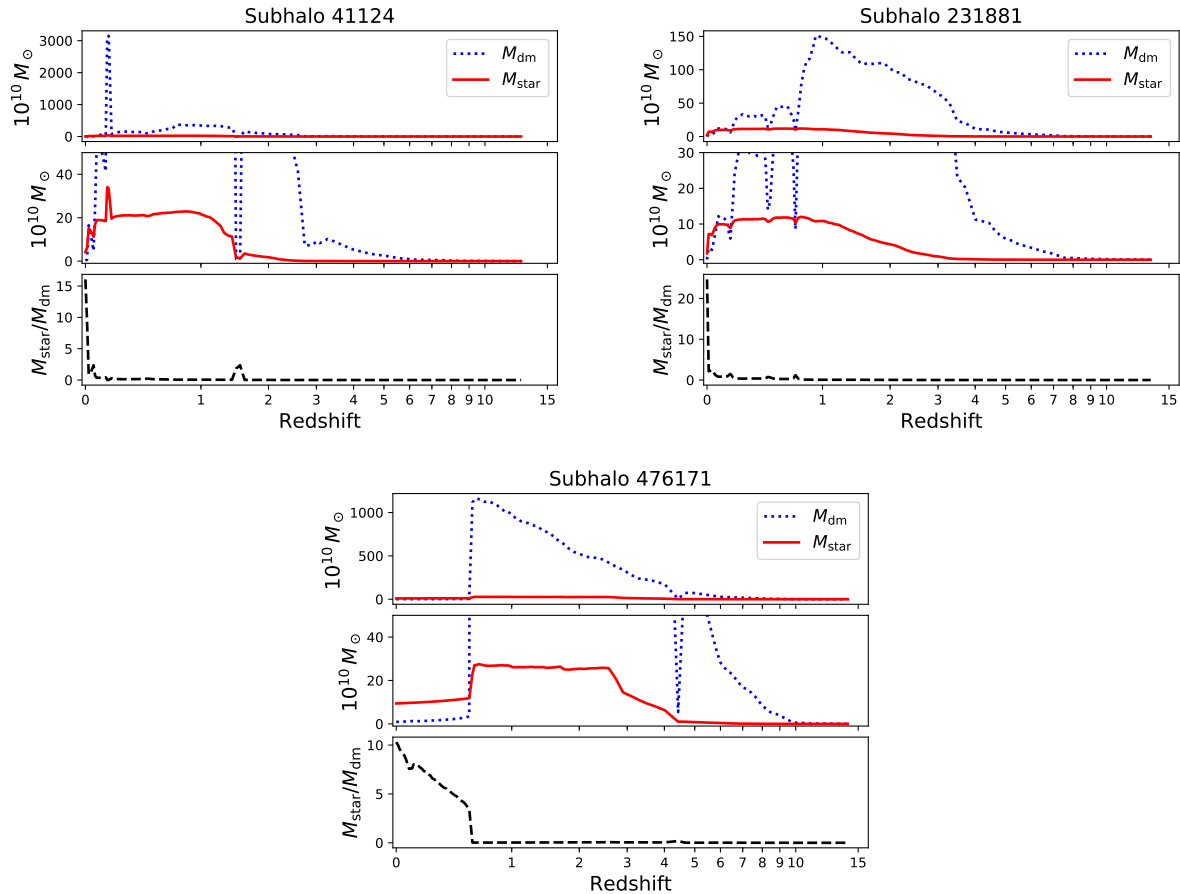


Figure 2. The mass history of the three massive dark matter deficient subhalos. Top subpanels are for dark matter and stars, middle subpanels zoom in on the lower mass region of the top subpanels, and bottom subpanels show the ratio $M_{\text{star}}/M_{\text{dm}}$. Note the drop in M_{star} and the deeper drop in M_{dm} at low redshift in the upper two subpanels for each of the three subhalos. This results in the relatively rapid increase in $M_{\text{star}}/M_{\text{dm}}$ for the subhalos at low redshift, seen in the lowest subpanel for each of the three subhalos.

ceased. Consistent with these properties, the mock images of these three subhalos show that they are elliptical subhalos (see Fig. 1). We trace the evolutionary history of these subhalos by using their sublink merger trees. We plot their dark matter mass and stellar mass histories in Fig. 2.⁸ All three subhalos have a period during which they rapidly lose most of their dark matter mass but lose relatively little of their stellar mass which results in abrupt increases of their $M_{\text{star}}/M_{\text{dm}}$ ratios. This might happen in a merger process of two large subhalos or through some other mechanism. After checking the evolutionary history of the three subhalos we find that both 41124 and 231881 are undergoing mergers. Subhalo 41124 is merging with subhalo 41089 and subhalo 231881 is merging with subhalo 231879 and the properties of these two new subhalos are also listed in Table 1. Subhalos 41089 and 231879 are much more massive than 41124 and 231881 and so dominate the merger processes and the two dark matter halos. If subhalos 41124 and 231881 can escape from their much more massive companions, they might form dark matter deficient galaxies. Subhalo 476171, whose stellar mass is $9.42 \times 10^{10} M_{\odot}$, comparable to that of our Milky Way, is an isolated elliptical galaxy and we will more closely examine its evolutionary history to understand how it formed.

Not all of the selected 307,786 SUBFIND subhalos with nonzero stellar mass are galaxies. Some of them, especially the less massive subhalos, are more likely to be substructures of other galaxies. To find subhalos that are galaxies, we check the ‘Parent’ property of each subhalo (the index in the subhalo table of the unique SUBFIND host subhalo of this

⁸ The histories plotted in Fig. 2 are assembled from that of the identified subhalo as well as its progenitor subhalo(s).

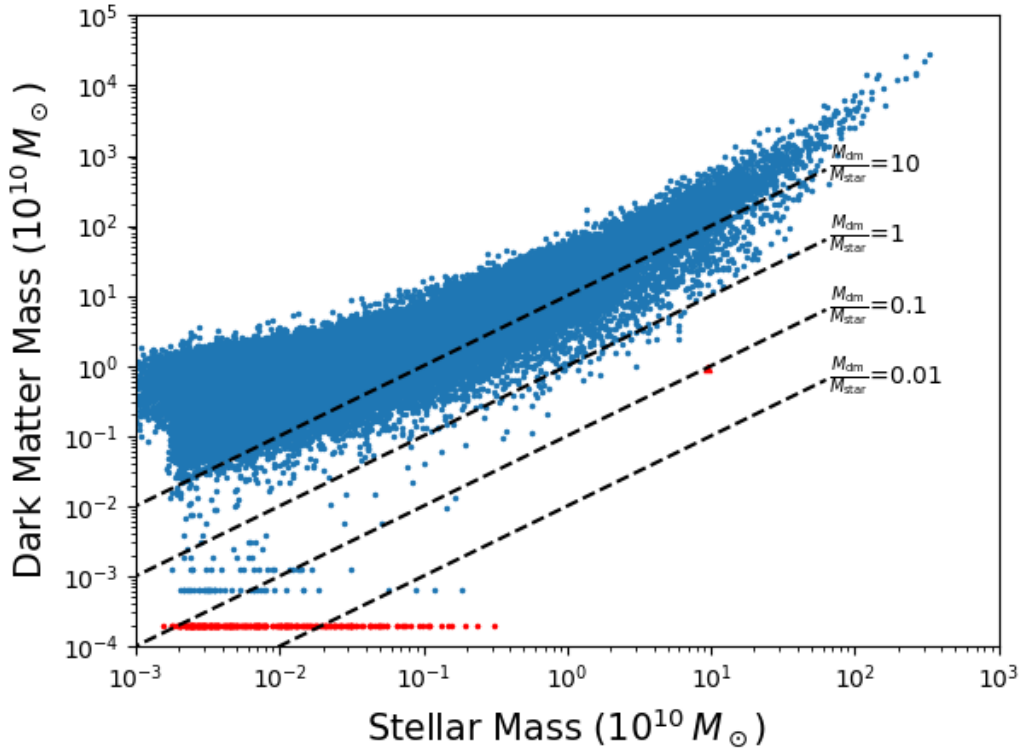


Figure 3. The distribution of the galaxy subhalo sample, with $M_{\text{star}} > 10^7 M_{\odot}$, in the stellar mass—dark matter mass plain. Blue points indicate subhalos and the inclined black dashed lines are loci of the ratio of subhalo dark matter to stellar mass. The lowest horizontal line of blue points correspond to subhalos with one dark matter particle and the lowest horizontal line of red points correspond to those subhalos without dark matter, moved here from $M_{\text{dm}} = 0$. The red star represents the massive subhalo 476171 ($M_{\text{star}} \approx 10^{11} M_{\odot}$) with $M_{\text{dm}}/M_{\text{star}} < 0.1$. (Masses here are SubhaloMassType masses.)

subhalo⁹) which can indicate if the subhalo of interest belongs to (is substructure in) a host subhalo. However, even if the value of the Parent index is 0 this could just mean that the host of the subhalo under consideration is just the most massive subhalo in the FoF group of the subhalo under consideration and not a separate galaxy. So we additionally compare the distance d between the subhalo under consideration and its host subhalo with the half-stellar-mass radius $r_{1/2}$, which contains half of the total stellar mass of the galaxy subhalo, of the host subhalo and regard the subhalo under consideration to be a galaxy only if it has $d > 2r_{1/2}$. We also discard subhalos with fewer than 20 stellar particles since half-stellar-mass radius is not measured as robustly for such objects. Applying these criteria, we get a new galaxy subhalo sample containing 58,025 subhalos that are galaxies. We will analyze this compilation in what follows.

Figure 3 shows the distribution of these galaxy subhalos as a function of their stellar mass and dark matter mass. Here we consider only the 57,945 galaxy subhalos with stellar mass larger than $10^7 M_{\odot}$. From the figure we find that there are some subhalos with $M_{\text{dm}}/M_{\text{star}}$ less than 1 which means these subhalos have more stellar mass than dark matter mass. There are 420 $M_{\text{dm}}/M_{\text{star}} < 1$ subhalos, which leads to a probability of about 0.72% for these $M_{\text{star}} > 10^7 M_{\odot}$ dark matter deficient subhalos. It is also clear that most of these have low stellar mass, less than $10^{10} M_{\odot}$.¹⁰ However, there is one subhalo with stellar mass greater than $10^{10} M_{\odot}$ and with $M_{\text{dm}}/M_{\text{star}} < 0.1$, shown as the red star in Fig. 3. This is subhalo 476171, discussed above, which we consider in more detail below. We also find that the other two dark matter deficient massive subhalos 41124 and 231881 discussed above do not appear in

⁹ This index is local to the FoF group. For example, index 2 indicates the third most massive subhalo of the parent halo of this subhalo, not the third most massive of the whole snapshot.

¹⁰ It is unclear what the galaxy subhalos with no dark matter (under SubhaloMassType), those indicated by the low red line of red points in Fig. 3, are. A few of the more massive ones have $M_{\text{star}} > 10^9 M_{\odot}$. We have looked at a few of the most massive of these but they only appear at $z = 0$ (snap 135) and so we are unable to trace their evolutionary history. They also do not have image data. It would be useful to understand how these galaxy subhalos formed and what observational constraints can be placed on them.

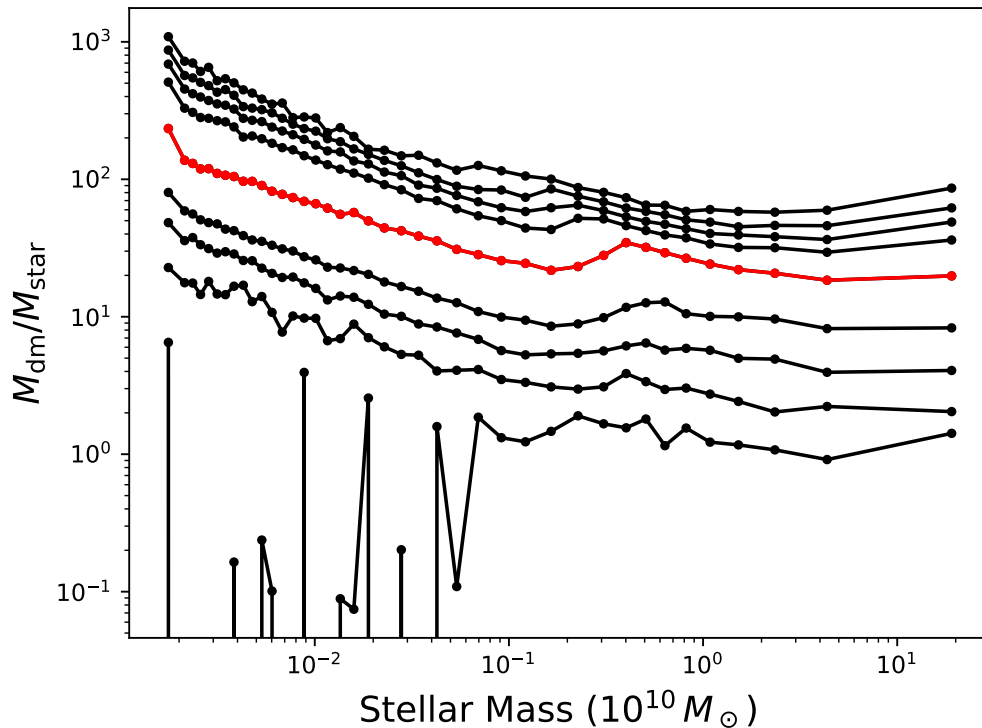


Figure 4. The ratio of dark matter mass to stellar mass as a function of stellar mass for the selected galaxy subhalo sample. (Masses here are SubhaloMassType masses.) The central red curve with dots is the median value and the outer black curves with dots represent the upper and lower 1σ , 1.5σ , 2σ , and 2.5σ confidence limits. The dots represent the mean stellar mass values in the bins. There are 40 bins and about 1450 objects in each bin.

this figure since they are participating in mergers and so are regarded as substructures of their much more massive companion galaxies. We emphasize that galaxy subhalo 476171 is an outlier, and also that it has many less extreme — but still very interesting — cousins with $M_{\text{star}} > 10^{10} M_{\odot}$ and $M_{\text{dm}}/M_{\text{star}} < 1$.

The relation between the $M_{\text{dm}}/M_{\text{star}}$ and M_{star} values of the galactic subhalos is shown in Fig. 4. From this figure we see that the median value of $M_{\text{dm}}/M_{\text{star}}$ spans a wide range, from about 20 to almost 300, and that this ratio decreases with increasing subhalo stellar mass. For given galaxy subhalo stellar mass, this ratio also spans a wide range, more so at the low stellar mass end. We see that the $M_{\text{dm}}/M_{\text{star}}$ lower 2.5σ limit curve lies at $M_{\text{dm}}/M_{\text{star}} \approx 1\text{--}3$ at the higher stellar mass end and, excluding some isolated bins, drops precipitously below about $M_{\text{star}} = 6 \times 10^8 M_{\odot}$. This result means that in the Λ CDM model there is some probability of forming galactic subhalos without or with only very little dark matter mass.

Since NGC1052-DF2 is said to be an ultra-diffuse galaxy, we also consider the half-stellar-mass radius, $r_{1/2}$, and plot the distribution of the galaxy subhalos in the $r_{1/2}$ —($M_{\text{dm}}/M_{\text{star}}$) plain, see Fig. 5. From this figure we see that, for say $M_{\text{dm}}/M_{\text{star}} \leq 5$, the half-stellar-mass radius $r_{1/2}$ decreases with decreasing galaxy subhalo mass ratio $M_{\text{dm}}/M_{\text{star}}$, if we ignore the red dots. Further, for $M_{\text{dm}}/M_{\text{star}} < 1$, there are some galaxy subhalos with relatively large half-stellar-mass radius, say > 2 kpc, which might appropriately be called ultra-diffuse galaxies. Figure 5 also shows that the Illustris simulation results in a few galaxy subhalos with $r_{1/2} > 50$ kpc. We examined their properties and found that they are the most or the second most massive galaxy subhalos in massive FoF groups, perhaps cD galaxies in galaxy clusters.¹¹ It is of interest to better understand these objects and to also observationally search for them in the real universe.

¹¹ Additionally, the left most red line of red dots in Fig. 5 corresponds to galaxy subhalos with no dark matter (under SubhaloMassType). Some of these have fairly large half-stellar-mass radius $r_{1/2}$, greater than a few kpc. It would be useful to understand how these galaxy subhalos formed and what observational constraints can be placed on them.

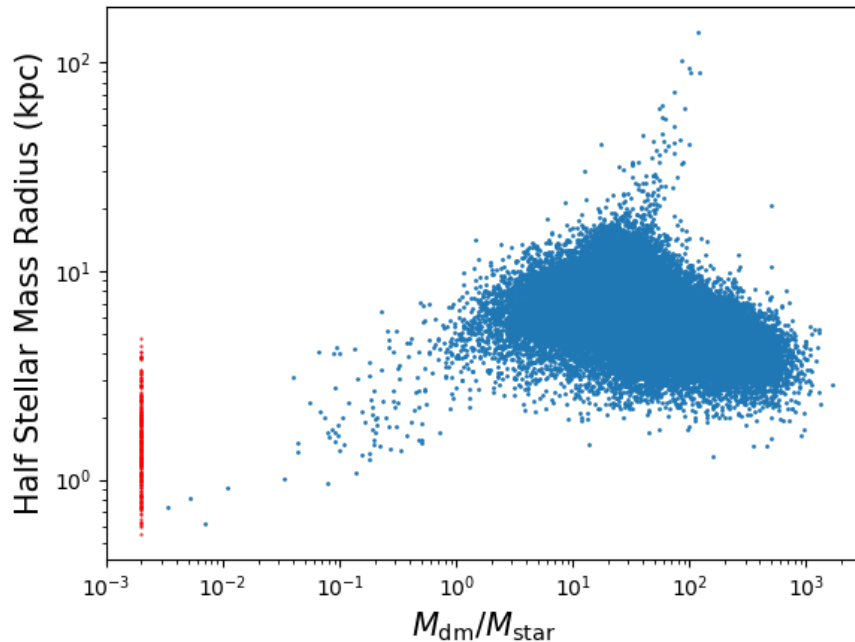


Figure 5. The distribution of the 57,945 galaxy subhalos with $M_{\text{star}} > 10^7 M_{\odot}$ in the $r_{1/2}$ —($M_{\text{dm}}/M_{\text{star}}$) plain. (Masses here are SubhaloMassType masses.) The left red line of red dots represent those subhalos with $M_{\text{dm}}/M_{\text{star}} = 0$, moved here from $M_{\text{dm}}/M_{\text{star}} = 0$. There are a number of galaxy subhalos in the $r_{1/2} > 2$ kpc and $M_{\text{dm}}/M_{\text{star}} < 1$ region; perhaps these might be called ultra-diffuse galaxies. We note the interesting galaxy subhalos with $r_{1/2} > 50$ kpc and $M_{\text{dm}}/M_{\text{star}} > 50$.

As noted above, Illustris SubhaloMassType masses are the total masses of all member particle/cells which are bound to the subhalo under consideration, separated by type. It is possible that some of the SubhaloMassType dark matter deficient galaxy subhalos we have found have diffuse dark matter halos whose masses do not contribute to M_{dm} computed using SubhaloMassType.¹² To examine this possibility we use the raw Illustris data of the 420 $M_{\text{dm}}/M_{\text{star}} < 1$ and $M_{\text{star}} > 10^7 M_{\odot}$ dark matter deficient galaxy subhalos (here M_{dm} and M_{star} are computed using SubhaloMassType).

From the raw data for each of the 420 galaxy subhalos we compute spherically symmetrized radial density profiles for the dark matter (dm), star, gas, and black hole (bh) particle distributions out to a radius of 50 kpc. See Figs. 6 and 7 for some examples. Most of these 420 galaxy subhalos have diffuse dark matter halos.

Only two (of the 420) have $M_{\text{dm}}/M_{\text{star}} < 1$ when the density profiles are integrated to a radial distance of 50 kpc from the galaxy subhalo center to determine M_{dm} and M_{star} . These are subhalos 476171 (center panel in the right hand column of Fig. 7) and 928035 (bottom panel in the left hand column of Fig. 7). We examined subhalo 928035 and found that it was an isolated small subhalo first seen at snap 135 ($z = 0$). Its main properties are listed in the last data row of Table 1. Since subhalo 928035 first appears at snap 135, it has no progenitor and we are unable to trace its history back in time and so do not know how it formed. We discuss the formation history of subhalo 476171 below.

Observationally, 50 kpc is not necessarily an appropriate distance to integrate to to determine whether a galaxy subhalo is dark matter deficient. Perhaps more reasonable is to integrate out to a small multiple of the galaxy subhalo half-stellar-mass radius $r_{1/2}$.¹³ If we integrate to $3r_{1/2}$ we find that 177 (of the 420 SubhaloMassType $M_{\text{dm}}/M_{\text{star}} < 1$ and $M_{\text{star}} > 10^7 M_{\odot}$) galaxy subhalos have raw data density profile $M_{\text{dm}}/M_{\text{star}} < 1$ and so are dark matter deficient. These 177 galaxy subhalos are 0.31% of the 57,945 Illustris galaxy subhalos with SubhaloMassType $M_{\text{star}} > 10^7 M_{\odot}$. Masses, $M_{\text{dm}}/M_{\text{star}}$'s, and density profiles for a dozen of these 177 subhalo galaxies are shown in Figs. 6 and 7.

¹² We thank V. Springel for pointing this out and for suggesting that we should also examine the raw Illustris data.

¹³ We use $r_{1/2}$ computed using SubhaloMassType as we are interested only in the star particles bound to the subhalo.

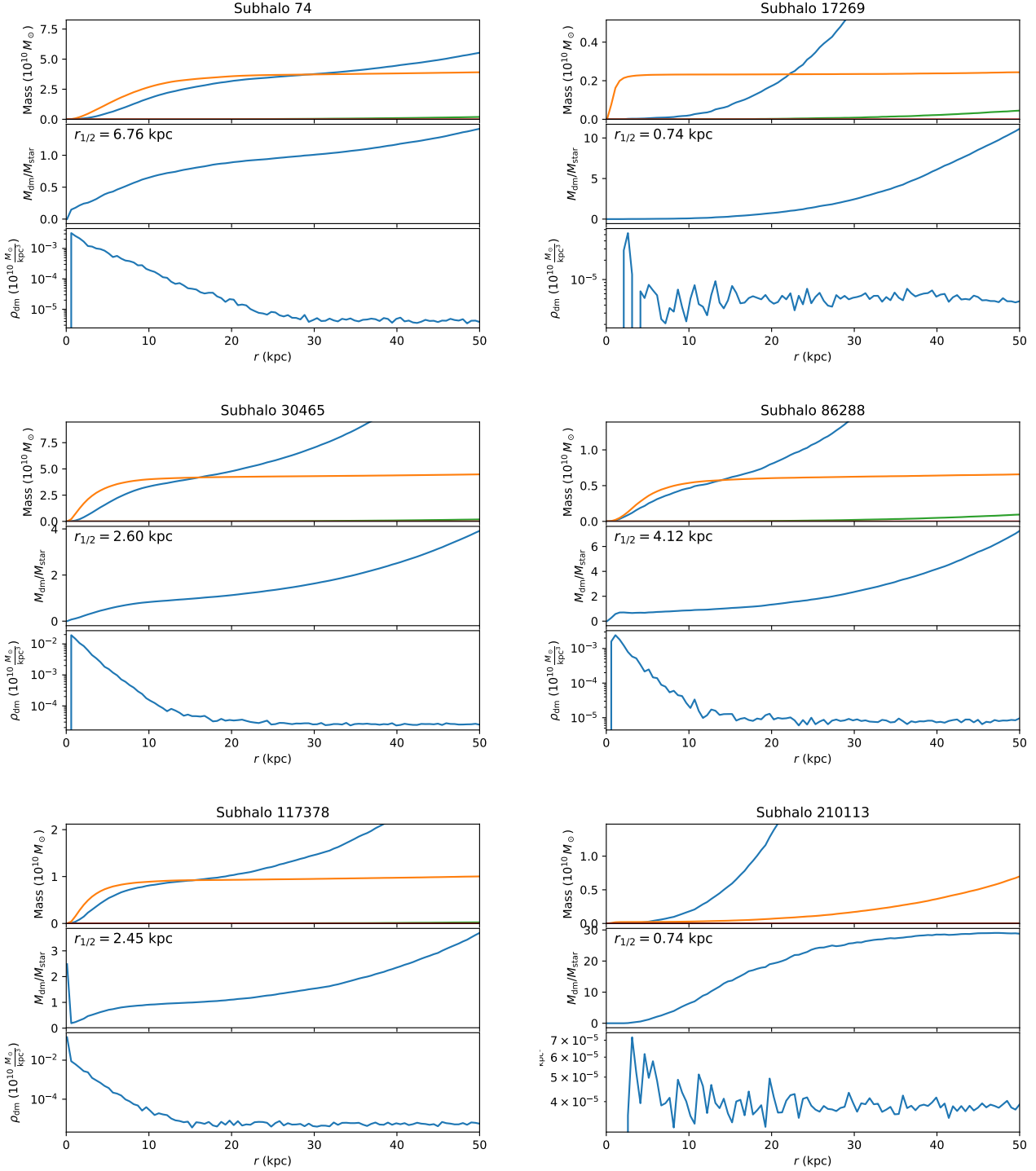


Figure 6. Density profiles of different particles for some dark matter deficient galaxy subhalos. Each panel title is the subhalo ID, and in each of the six panels the top subpanel shows the various masses within $< r$ (linestyles are defined in the top subpanel of the top-left panel), the middle subpanel shows the $M_{\text{dm}}/M_{\text{star}}$ within $< r$, and the bottom subpanel shows the density of dark matter at radius r . $r_{1/2}$ values listed in the middle subpanels are half-stellar-mass radii computed using SubhaloMassType.

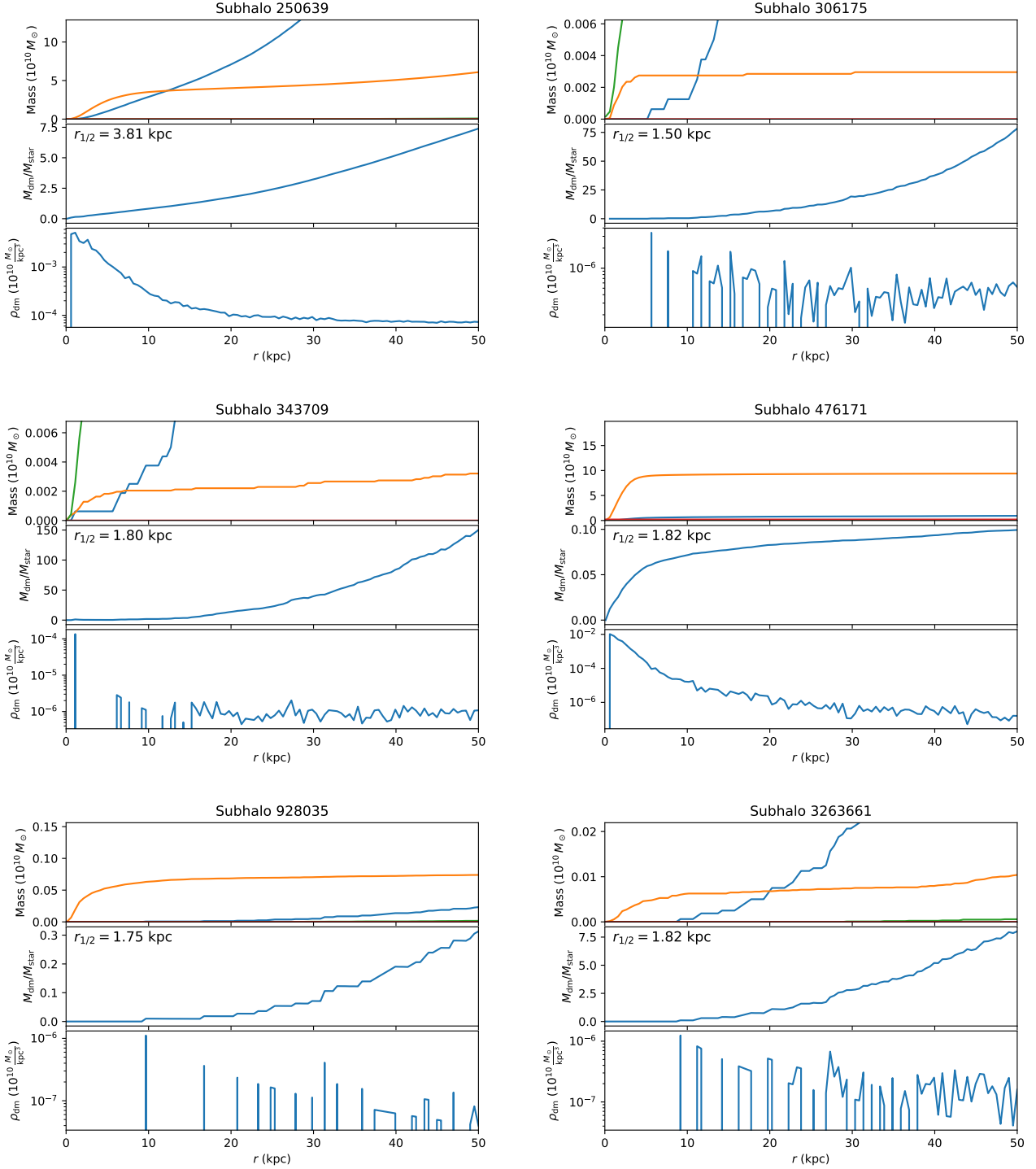


Figure 7. See Fig. 6 caption.

The distribution of these 177 subhalo galaxies as a function of stellar mass is shown in Fig. 8. Figure 9 shows the distribution of these 177 galaxy subhalos in the $r_{1/2} - (M_{\text{dm}}/M_{\text{star}})$ plane.

Figure 8 shows that the distribution in stellar mass of the 177 dark matter deficient galaxy subhalos is reasonably flat. It is of significant interest to determine the relative probability of these 177 subhalos as a function of stellar mass. A proper computation of this probability requires a determination of $M_{\text{dm}}/M_{\text{star}}$ from the density profiles of all 57,945

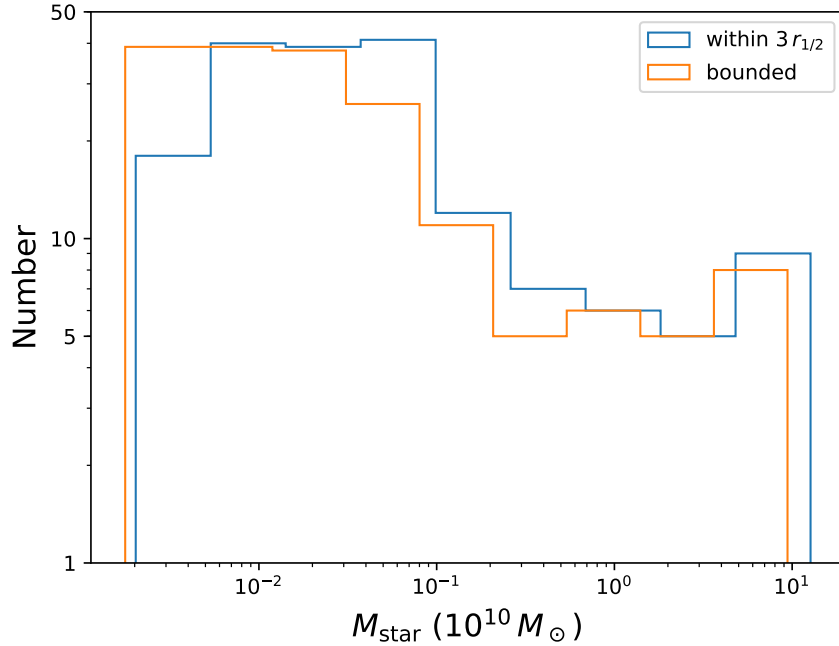


Figure 8. Distribution of the 177 dark matter deficient galaxy subhalos as a function of stellar mass. Blue histogram is for M_{star} computed by integrating the star particle density profile to $3r_{1/2}$ while the orange histogram is for SubhaloMassType M_{star} .

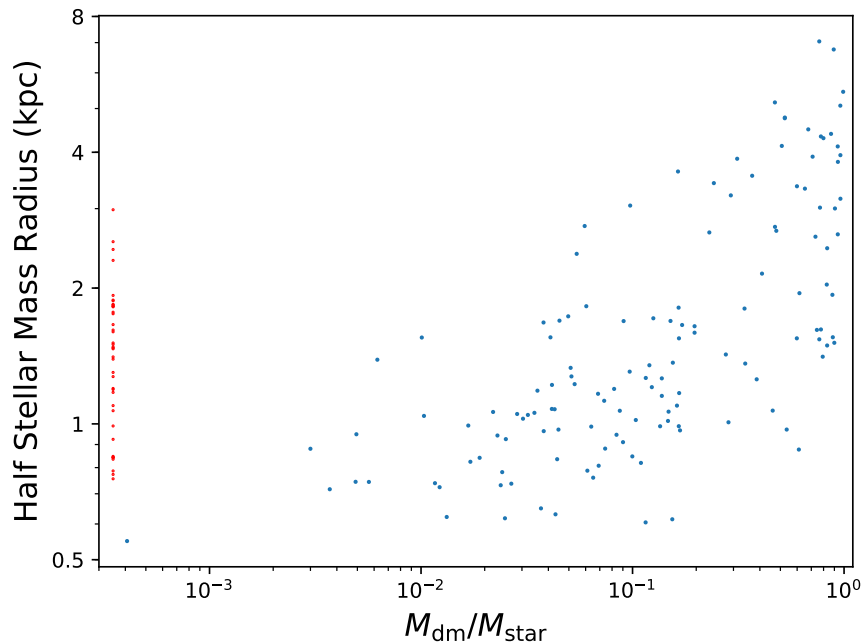


Figure 9. Same as Fig. 5 but now for only the 177 dark matter deficient galaxy subhalos, with $M_{\text{dm}}/M_{\text{star}}$ determined from an integration of the density profiles to $3r_{1/2}$. Perhaps the 47 (26.6% of 177) galaxy subhalos in the $r_{1/2} > 2$ kpc and $M_{\text{dm}}/M_{\text{star}} < 1$ region might be called ultra-diffuse galaxies. Note that there still are some galaxy subhalos with no dark matter (the red dots), although many fewer than those in Fig. 5.

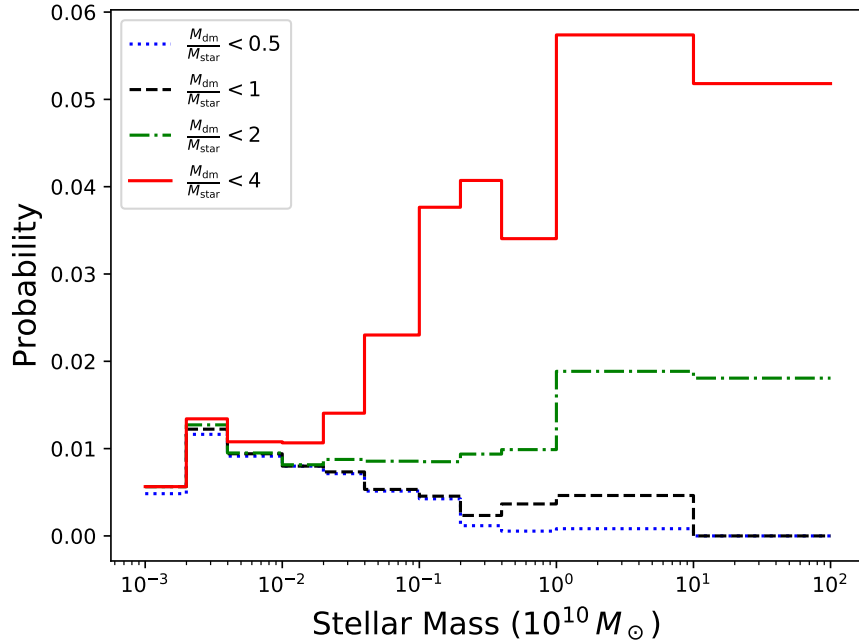


Figure 10. Fractional number of galaxy subhalos satisfying the indicated SubhaloMassType $M_{\text{dm}}/M_{\text{star}}$ constraint, relative to the total number of subhalos in the corresponding stellar mass bin. See Table 2 for numerical values.

galaxy subhalos with $M_{\text{star}} > 10^7 M_{\odot}$. This is beyond the computer resources we have available. We have found that 42% of the SubhaloMassType $M_{\text{dm}}/M_{\text{star}} < 1$ galaxy subhalos are indeed dark matter dominated when we integrate the density profiles to $3r_{1/2}$ (177 out of 420).¹⁴ Consequently $M_{\text{dm}}/M_{\text{star}}$ determined using SubhaloMassType is likely to provide a qualitatively reasonable approximation of the more correct $M_{\text{dm}}/M_{\text{star}}$ determined from an integration of the density profiles and so we use the SubhaloMassType $M_{\text{dm}}/M_{\text{star}}$'s to qualitatively estimate the relative probability (an estimate that should be correct to within a factor of 2 or 3).

Figure 10 and Table 2 show and list the relative probabilities of dark matter deficient (under SubhaloMassType) galaxy subhalos in a range of stellar mass bins. We see that more than 0.7% of galaxy subhalos with SubhaloMassType $M_{\text{star}} \approx 2 \times 10^8 M_{\odot}$ (as found for the ultra-diffuse dwarf galaxy NGC1052-DF2 by van Dokkum et al. 2018a) have SubhaloMassType $M_{\text{dm}}/M_{\text{star}} < 1$. Even for galaxies with $M_{\text{star}} \approx 10^9 M_{\odot}$, which should be easier to see, more than 0.4% have $M_{\text{dm}}/M_{\text{star}} < 0.5$. If Λ CDM and the Illustris simulation are accurate, given these SubhaloMassType probabilities, perhaps the more surprising thing about NGC1052-DF2 is not the low $M_{\text{dm}}/M_{\text{star}}$ but rather that it took so long to find the first dark matter deficient galaxy (if it is indeed confirmed as such).

We now consider in more detail the massive dark matter deficient galaxy subhalo 476171. In snap 135 at $z = 0$, subhalo 476171 is isolated with no satellite subhalo or substructure. Its half-stellar-mass radius is 1.82 kpc and its stellar photometric radius¹⁵ is 4.76 kpc. Galaxy subhalo 476171 is very small relative to its large stellar mass and so the stars in 476171 are bound together tightly.¹⁶ From Table 1 we see that the other two massive dark matter deficient subhalos are also relatively small.

Galaxy subhalo 476171 has a three-dimensional velocity dispersion of 280 km s^{-1} and a black hole of mass $\approx 2 \times 10^9 M_{\odot}$. These values are only a little smaller than those that have been used to define massive ultracompact galaxies (MUGs, Buitrago et al. 2018). To establish whether 476171 can actually be classified as a MUG is beyond the

¹⁴ This ratio will depend on the distance to which the density profiles are integrated, also, for the following M_{star} -bins discussion, the ratio will depend on the value of M_{star} under consideration.

¹⁵ The radius at which the surface brightness profile, computed from all member stellar particles, drops below the limit of $20.7 \text{ mag arcsec}^{-2}$ in the K band.

¹⁶ It is possible that at least the more massive dark matter deficient galaxy subhalos (with $M_{\text{dm}}/M_{\text{star}} < 1$ and $M_{\text{star}} > 10^{10} M_{\odot}$, see Fig. 3) have to be more tightly bound and hence might be expected to be ellipticals. Given their small spatial extent they should have higher surface brightness than more normal dark matter dominated galaxies of the same stellar mass. As a result they will likely not look like more normal dark matter dominated galaxies. It is of interest to determine what observational limits exist on such dark matter deficient galaxies and it is also of interest to search for such galaxies.

| Stellar mass ($10^{10} M_{\odot}$) bin | Total number of subhalos | Subhalos with $M_{\text{dm}}/M_{\text{star}}$ | | | | | | | |
|--|--------------------------|---|-----|-----|-----|-------------|-------|-------|-------|
| | | Number | | | | Probability | | | |
| | | < 0.5 | < 1 | < 2 | < 4 | < 0.5 | < 1 | < 2 | < 4 |
| $[1,2) \times 10^{-3}$ | 1240 | 6 | 7 | 7 | 7 | 0.48% | 0.56% | 0.56% | 0.56% |
| $[2,4) \times 10^{-3}$ | 10142 | 118 | 124 | 129 | 136 | 1.16% | 1.22% | 1.27% | 1.34% |
| $[0.4,1) \times 10^{-2}$ | 10946 | 100 | 103 | 104 | 118 | 0.91% | 0.94% | 0.95% | 1.08% |
| $[1,2) \times 10^{-2}$ | 6380 | 51 | 51 | 52 | 68 | 0.80% | 0.80% | 0.82% | 1.07% |
| $[2,4) \times 10^{-2}$ | 4909 | 35 | 36 | 43 | 69 | 0.71% | 0.73% | 0.88% | 1.41% |
| $[4,10) \times 10^{-2}$ | 5258 | 27 | 28 | 45 | 121 | 0.51% | 0.53% | 0.86% | 2.30% |
| $[0.1,0.2)$ | 3294 | 14 | 15 | 28 | 124 | 0.43% | 0.46% | 0.85% | 3.76% |
| $[0.2,0.4)$ | 3414 | 4 | 8 | 32 | 139 | 0.12% | 0.23% | 0.94% | 4.07% |
| $[0.4,1)$ | 5463 | 3 | 20 | 54 | 186 | 0.05% | 0.37% | 0.99% | 3.40% |
| $[1,10)$ | 6047 | 5 | 28 | 114 | 347 | 0.08% | 0.46% | 1.89% | 5.74% |
| $[10,100]$ | 830 | 0 | 0 | 15 | 43 | 0.00% | 0.00% | 1.81% | 5.18% |

Table 2. Census of galaxy subhalos in different stellar mass bins. Masses are SubhaloMassType masses.

scope of this paper. It is also of interest to measure the stellar and dynamical masses of MUGs to determine whether some or all them are dark matter deficient galaxies.

To understand how galaxy subhalo 476171 formed, we trace its formation history by examining the cutouts (which give the matter distribution and properties, such as the positions and velocities of the gas, dark matter and star particles, of its progenitors and parent groups) in snap 54 to 103 (from $z = 4.01$ to 0.5) and in snap 134 ($z = 0.01$) and 135 ($z = 0$). Figure 11 plots the cutout data of 476171 and its parent groups in a dozen snaps. The gray dots represent dark matter particles, purple dots stars, blue circles subhalos (with circle area proportional to stellar mass), and blue arrows represent the velocities of the five most massive subhalos in the parent groups. The red circles identify the progenitors of 476171 in the different snaps, the red dots are the positions of the stars which finally end up in subhalo 476171 in snap 135, and red arrows represent the mean velocity of the red stars. From these figures we see that at first the subhalo is at the center of its parent group that has a very large dark matter halo and they largely move together in the positive x direction. But in snap 85 ($z = 1.0$), the subhalo has ceased moving in the positive x direction while the rest of the group largely continues to do so. The subhalo then moves slowly towards the edge of the dark matter halo although it still dominates the whole halo until snap 100 ($z = 0.58$) when a new subhalo starts forming at the center of the dark matter halo. This new subhalo comes to dominate the rest of the dark matter while the progenitor subhalo of 476171 is now at the edge of the whole dark matter halo and continues to move outwards. By this point the progenitor subhalo of 476171 has lost most of its dark matter and some (although relatively less) of its stellar mass which results in it becoming a dark matter deficient galaxy subhalo. (See the lower redshift parts of the central and lower subpanels in the subhalo 476171 panel of Fig. 2.) It keeps moving outward, getting farther and farther away from the rest of the dark matter halo. By snap 135 at $z = 0$, it has completely escaped from its former parent group, forming an isolated group of one with much more stellar mass than dark matter mass.

It is important to more clearly understand the physical processes that caused the ejection of galaxy subhalo 476171, as well as those that played a role in causing it to become dark matter deficient. We do not yet have a satisfactory understanding of either of these. In an attempt to elucidate what took place we focus on the progenitor(s) of galaxy subhalo 476171 and the second most massive nearby galaxy subhalo, whose SUBFIND ID is 78979 in snap 80 ($z = 1.21$), and follow these to snap 110 ($z = 0.38$). Eighteen snaps between 80 and 110 are shown in Figs. 12 and 13. For clarity these figures show only the more centrally concentrated stellar particles. In these two groups of figures, the green dots represent the stellar particles of subhalo 78979 and its descendants, the red dots are the stellar particles which will leave the FoF group and eventually end up in the subhalo 476171, and the blue dots (along with the red dots) are the stellar particles in the progenitors of galaxy subhalo 476171. (At snap 99 the blue and red dots belong to subhalo 143860, after snap 100 most of the blue dots belong to another subhalo, subhalo 155159 at snap 101.) The green, red, and black arrows are the velocities of the green, red, and blue collections of stars. The arrow in the top-left panels of

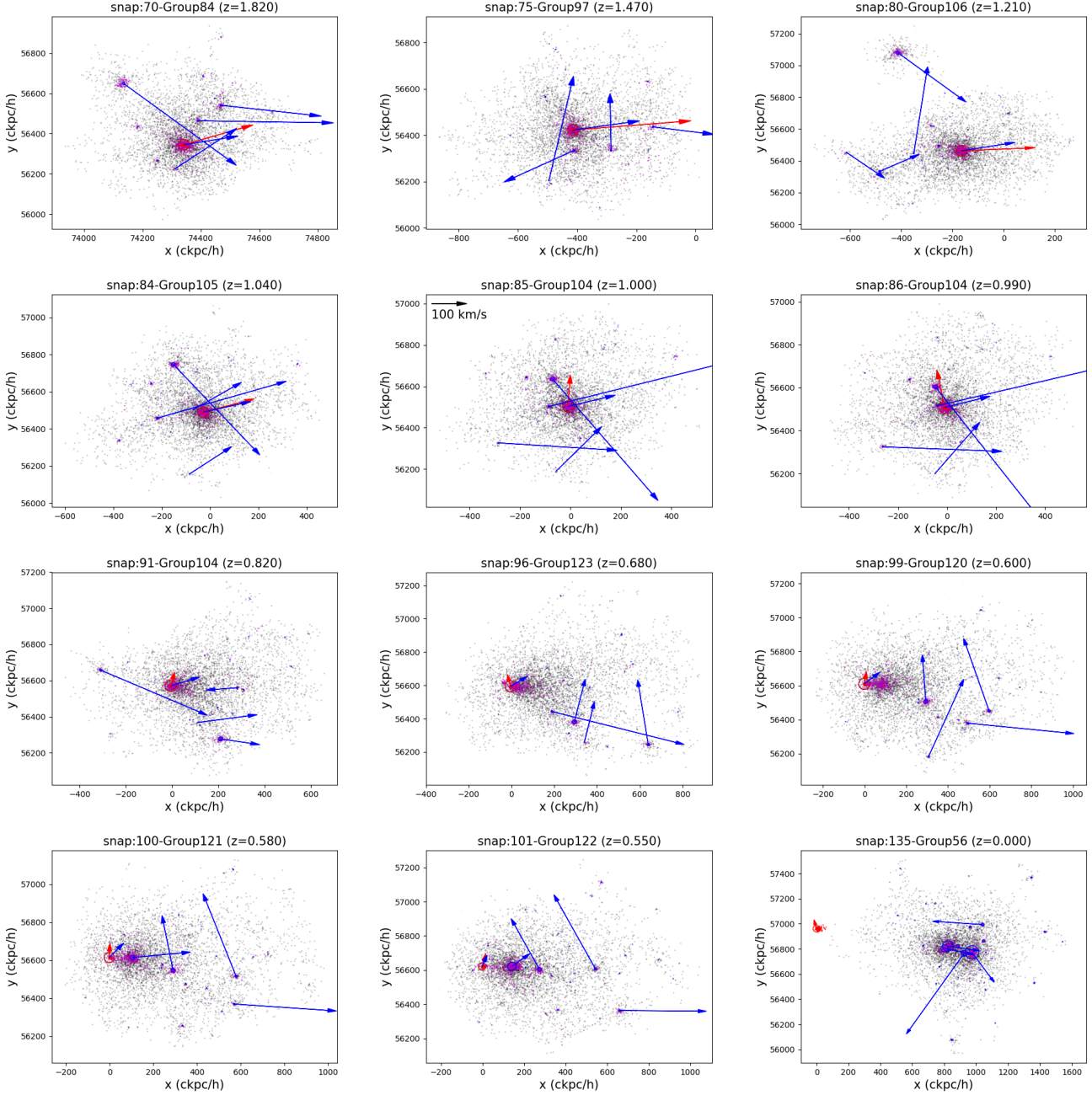


Figure 11. The evolutionary history of subhalo 476171. See text for information about symbols. Distance units are comoving kpc/h where $h = 0.704$. The arrow in the top-left corner of the central panel in the second row indicates the velocity scale.

Figs. 12 and 13 shows the velocity scale. In each panel we also list the snap number, the redshift, and the stellar mass (in units of $10^{10} M_{\odot}$) of each of the three star clumps (in three different colors). Table 3 lists these and other relevant masses.¹⁷

¹⁷ In Figs. 12 and 13 and Table 3 the listed masses are determined by summing together the masses of all the particles of interest. These are not SubhaloMassType masses, although they do not appreciably differ from SubhaloMassType masses when both can be computed. We note that unlike SubhaloMassType masses, where gas masses include wind particle masses, in our procedure wind particle masses are included with star masses. (Wind particle masses do not contribute significantly to the totals.) We need to use our procedure for the mass determination (instead of using SubhaloMassType) because we want to follow the red stellar mass that eventually ends up in subhalo 476171 from well before the time when subhalo 476171 came into existence.

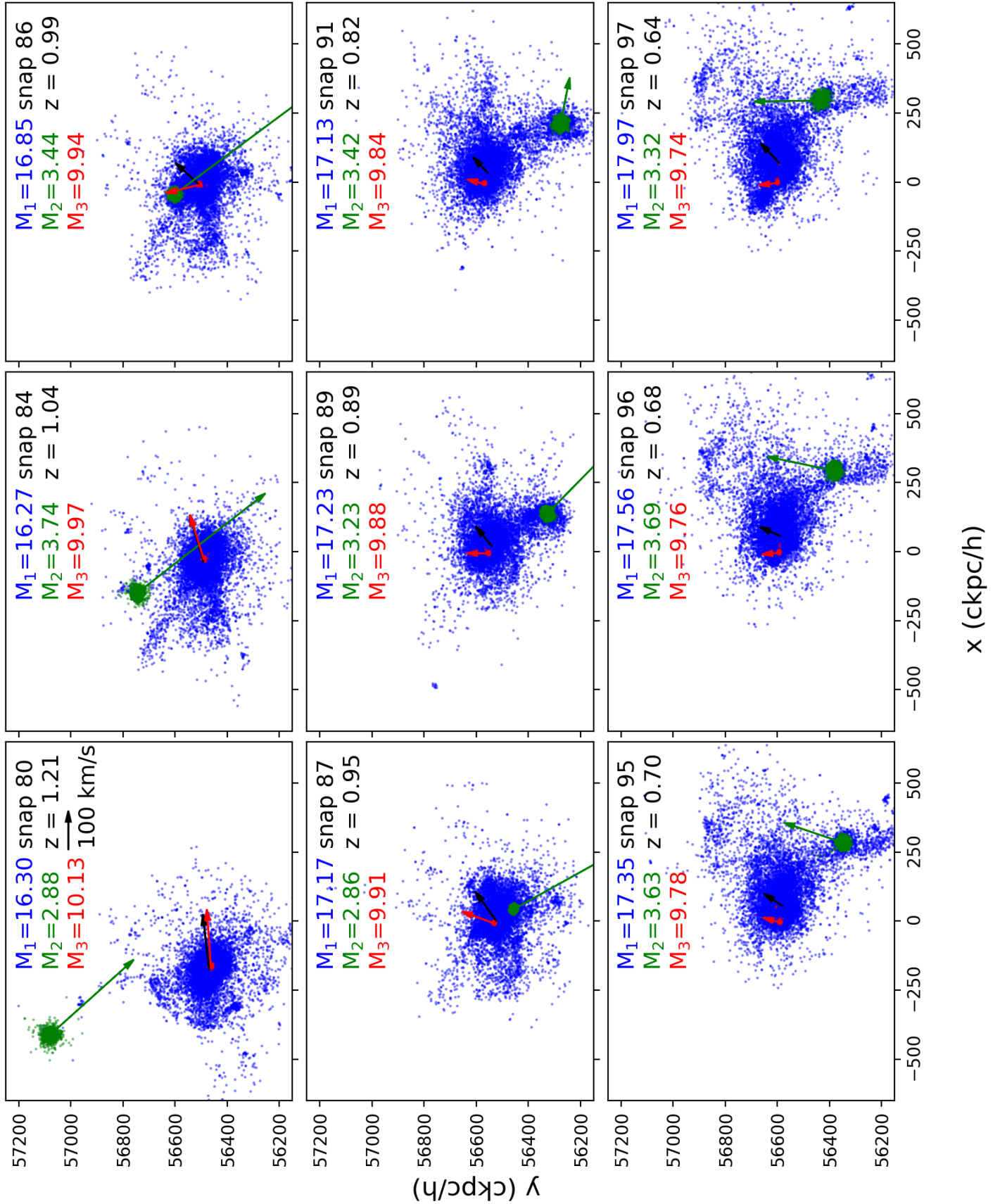


Figure 12. The stellar evolutionary history of subhalo 476171 and its progenitors, from snap 80 to 97. See text for information about symbols. Distance units are comoving kpc/h where $h = 0.704$.

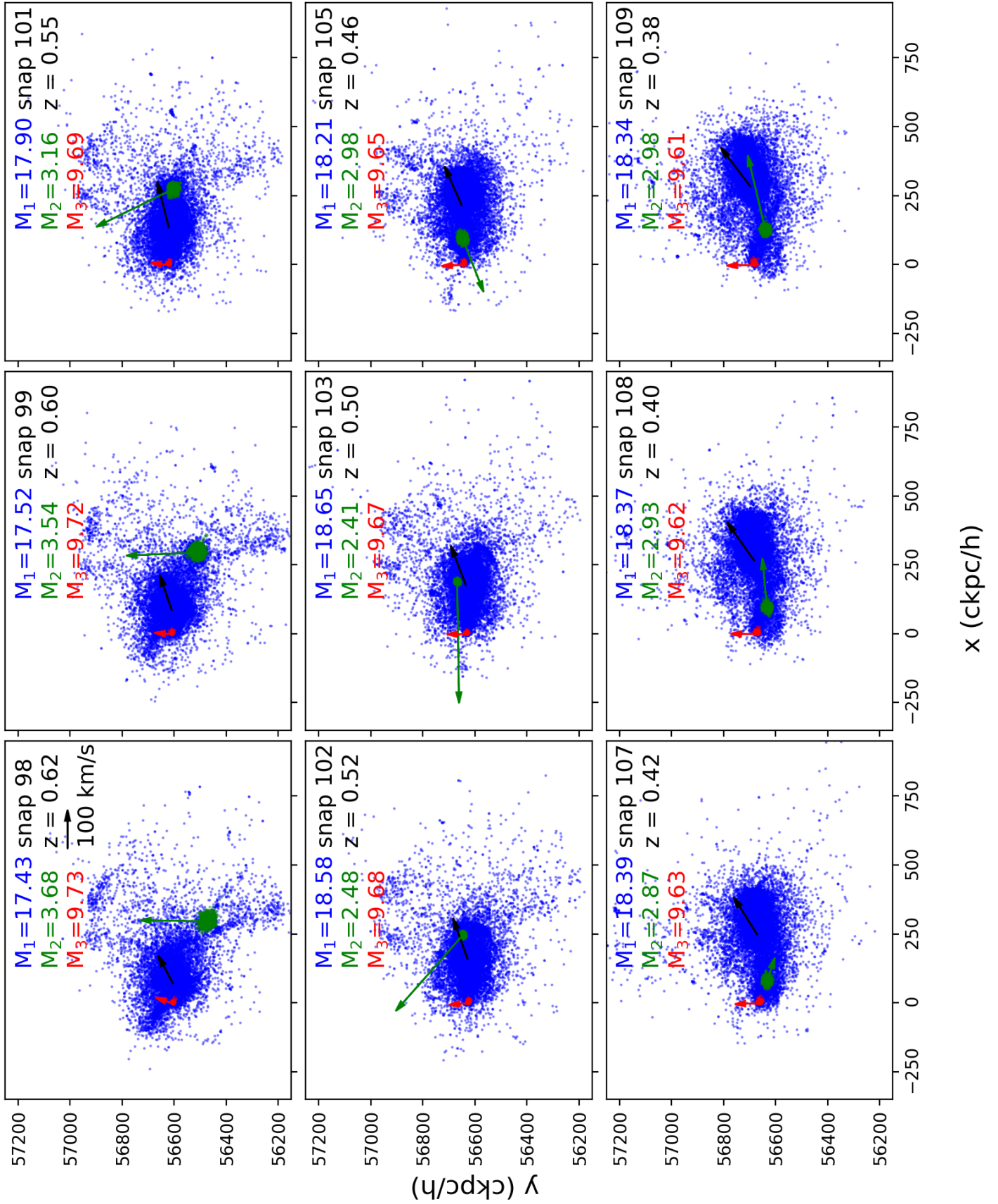


Figure 13. Same as Fig. 12 but now from snap 98 to 109.

From these figures we see that the green and red+blue subhalos participate in a significant and protracted interaction.¹⁸ The first part of this interaction, during snaps 84 to 89, results in the braking of the positive x direction motion of the red clump relative to the blue stellar particles. Given the length scales involved it is reasonable to assume that the gravitational force is the main cause of the relative motion of the green and red+blue stars and also of the relative motion between the red clump and the blue stars. See Table 3 for the masses involved in these motions. It seems that as the green clump comes in to the red+blue halo (see snaps 84 and 86) it initially more successfully pulls the compact red clump to it, compared to the effect it has on the more diffuse blue star collection (which it distorts by more effectively pulling closer blue stars towards it), and this gives rise to an overall relative velocity between the red and blue star particles.

By snap 95 ($z = 0.70$), the green subhalo has almost turned around and as it moves back farther into the red+blue subhalo it has a bigger effect on the nearer blue particles (the red clump is now farther away), pulling them towards it and causing the blue particles to accelerate in the positive x direction and away from the red clump. Until about snap 103 ($z = 0.5$) the green subhalo is on the right of, and closer to, the center of the blue stars and so continues to more effectively pull blue stars away from the red clump. The green subhalo continues to move in a counterclockwise direction and during snaps 104 to 109 it is between the red clump and the center of the blue stars and no longer seems to increase the relative velocity between the blue and red clumps, however by this time the relative velocity is large enough for the red clump to go its own way and escape from the blue clump.

This behavior is also apparent in the redshift evolution of the velocity differences between the red, blue, and green clumps, see Fig. 14.¹⁹ We see that as the green clump of stars makes a first pass through the central region of the red+blue clump of stars during redshifts between about 1 and 0.9, which correspond to snaps 86 and 89, the x component of the red and blue velocity difference (the solid blue line in Fig. 14) deviates away from zero to the negative side, because the green clump is more effectively pulling the blue stars towards it. As the green clump continues to move outwards the differential effect it has on the red and blue clumps presumably decreases, resulting in a decrease of the velocity difference between the red and blue clumps. By snap 95 ($z = 0.7$) the green clump has turned around and starts moving in a counterclockwise direction. As it comes back in it is on the right side of the blue clump and closer to it than to the red clump, presumably pulling more effectively on the blue clump than on the red clump and so increasing the x component of the velocity difference between the blue and red clumps, that by snap 99 ($z = 0.6$) has settled down to around 100 km/s, with the red stars drifting away in the negative x direction from the blue stars.

It seems reasonable, at the level of the big picture, to presume that the tidal effects of gravity are responsible for both the red clump being ejected and for it becoming dark matter deficient, and that the interaction between the green and red+blue clumps was the prime cause of both, with the compactness of the red clump presumably also playing an important role. It is however very desirable to have a better and more granular understanding of this phenomenon, which might require a local simulation with higher resolution.

Table 3 lists masses of these objects from snap 80 to 110 (we do not record black hole particle masses here as these are much smaller). While the green clump is relatively much less massive than the red+blue one (it is only 6% as massive at snap 80), they have a reasonably high relative velocity, and the green clump loses most of its dark matter while interacting with the red+blue one. So it seems likely that gravity has enough to work with to be able to eject the red clump while stripping it of most of its dark matter and a significant amount of its stellar matter, thus creating a massive dark matter deficient galaxy (subhalo 476171).

Interestingly, if galaxy subhalo 476171 is a MUG, then perhaps the formation process we have summarized here can explain how some MUGs can come to exist in low-density environments (Buitrago et al. 2018). Observationally determining the dark matter fraction of MUGs as a function of environment might allow for discrimination between different MUG formation channels (Buitrago et al. 2018).

3. CONCLUSION

Motivated by the findings of van Dokkum et al. (2018a), we have searched for dark matter deficient galaxy subhalos in the Illustris simulation (www.illustris-project.org, Vogelsberger et al. 2014a) of the Λ CDM cosmogony and have discovered a significant number that seem to have properties similar to those ascribed to ultra-diffuse galaxy NGC1052-DF2 by van Dokkum et al. (2018a). It is of interest to more carefully examine such galaxy subhalos in the Illustris

¹⁸ By also viewing the x - z projections of snaps 80 to 110 we have verified that the green subhalo passes through the red+blue subhalo.

¹⁹ We thank J. Peebles for suggesting that we examine these velocity differences.

| Snap (Redshift) | Red+Blue | | | Blue SW | Red SW | Green | | |
|-----------------|----------|------|-------|---------|--------|-------|------|------|
| | Gas | DM | SW | | | Gas | DM | SW |
| 80 (1.21) | 17.2 | 876 | 26.4 | 16.3 | 10.1 | 9.81 | 42.5 | 2.88 |
| 81 (1.15) | 18.7 | 892 | 26.3 | 16.2 | 10.1 | 9.49 | 37.5 | 3.22 |
| 82 (1.11) | 19.8 | 901 | 26.3 | 16.2 | 10.1 | 9.05 | 35.5 | 3.33 |
| 83 (1.07) | 22.5 | 929 | 26.2 | 16.2 | 10 | 7.18 | 26.2 | 3.51 |
| 84 (1.04) | 25.2 | 942 | 26.27 | 16.3 | 9.97 | 6.05 | 23.2 | 3.74 |
| 85 (1) | 29.6 | 975 | 26.34 | 16.4 | 9.94 | 3.97 | 15.8 | 3.67 |
| 86 (0.99) | 31.6 | 988 | 26.74 | 16.8 | 9.94 | 2.9 | 11.3 | 3.44 |
| 87 (0.95) | 35 | 1010 | 27.11 | 17.2 | 9.91 | 1.87 | 5.69 | 2.86 |
| 88 (0.92) | 34 | 1010 | 27 | 17.1 | 9.9 | 3.31 | 8.13 | 3.17 |
| 89 (0.89) | 37.1 | 1040 | 27.08 | 17.2 | 9.88 | 2.23 | 7.64 | 3.23 |
| 90 (0.85) | 38.7 | 1070 | 27.06 | 17.2 | 9.86 | 3.11 | 8.17 | 3.37 |
| 91 (0.82) | 41.5 | 1100 | 26.94 | 17.1 | 9.84 | 1.98 | 8.39 | 3.42 |
| 92 (0.79) | 43 | 1110 | 26.93 | 17.1 | 9.83 | 2.45 | 8.73 | 3.49 |
| 93 (0.76) | 23.4 | 1120 | 26.91 | 17.1 | 9.81 | 2.67 | 9.26 | 3.51 |
| 94 (0.73) | 11.3 | 1130 | 27.09 | 17.3 | 9.79 | 3.24 | 8.94 | 3.51 |
| 95 (0.7) | 11.5 | 1120 | 27.18 | 17.4 | 9.78 | 3.57 | 8.98 | 3.63 |
| 96 (0.68) | 12.4 | 1130 | 27.36 | 17.6 | 9.76 | 2.1 | 10.1 | 3.69 |
| 97 (0.64) | 13.8 | 1150 | 27.74 | 18 | 9.74 | 1.06 | 8.23 | 3.32 |
| 98 (0.62) | 14.7 | 1160 | 27.13 | 17.4 | 9.73 | 1.29 | 10.7 | 3.68 |
| 99 (0.6) | 14.8 | 1160 | 27.22 | 17.5 | 9.72 | 0.935 | 9.41 | 3.54 |
| 100 (0.58) | 14.9 | 1110 | 23.11 | 13.4 | 9.71 | 0.781 | 7.85 | 3.32 |
| 101 (0.55) | 15.9 | 1160 | 27.59 | 17.9 | 9.69 | 0.81 | 6.49 | 3.16 |
| 102 (0.52) | 16.7 | 1190 | 28.28 | 18.6 | 9.68 | 0.601 | 3.6 | 2.48 |
| 103 (0.5) | 16.8 | 1190 | 28.37 | 18.7 | 9.67 | 0.737 | 3.28 | 2.41 |
| 104 (0.48) | 17.5 | 1220 | 27.86 | 18.2 | 9.66 | 0.606 | 4.99 | 2.92 |
| 105 (0.46) | 17.3 | 1240 | 27.85 | 18.2 | 9.65 | 0.48 | 5.25 | 2.98 |
| 106 (0.44) | 18.9 | 1270 | 27.94 | 18.3 | 9.64 | 0.458 | 4.95 | 2.89 |
| 107 (0.42) | 20.5 | 1310 | 28.03 | 18.4 | 9.63 | 0.51 | 4.88 | 2.87 |
| 108 (0.4) | 19.1 | 1330 | 28.02 | 18.4 | 9.62 | 0.56 | 5.13 | 2.93 |
| 109 (0.38) | 20.5 | 1370 | 27.91 | 18.3 | 9.61 | 0.563 | 5.34 | 2.98 |
| 110 (0.36) | 22.1 | 1400 | 27.9 | 18.3 | 9.6 | 0.575 | 5.46 | 3.03 |

Table 3. Gas, dark matter (DM), and star + wind (SW) masses (in units of $10^{10} M_{\odot}$) of the red+blue and green clumps, as well as the star + wind masses of the blue and red clumps from snap 80 to 110. (Stellar mass dominates the star + wind masses.) The “Red+Blue” columns give the masses of different particles in the subhalo (subhalos after snap 100) which the red and blue stellar particles belong to and the “Green” columns give the masses of different particles in the subhalo which the green stars belong to. The “Blue SW” and “Red SW” columns are the sum of masses of the blue dots and red dots in Figs. 12 and 13.

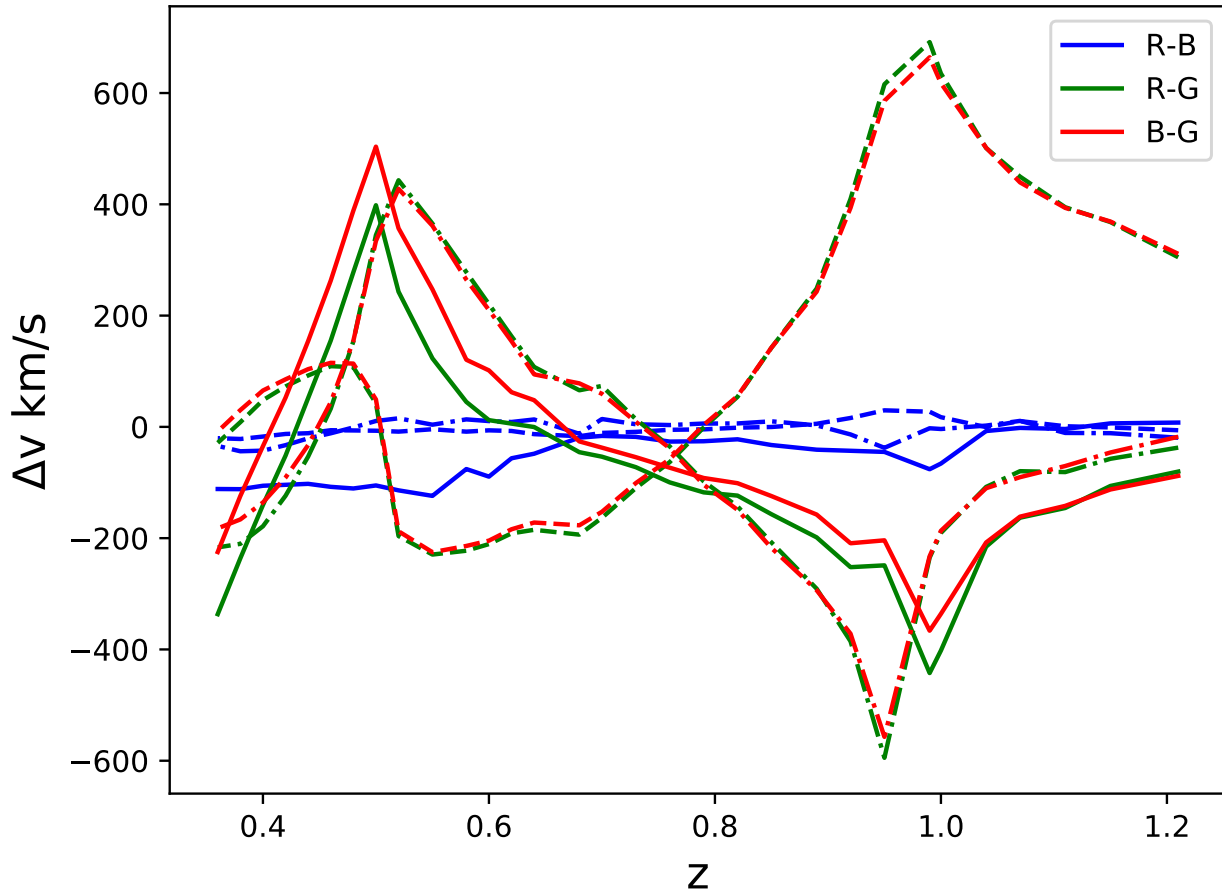


Figure 14. Redshift evolution of the velocity differences between the red, blue, and green collections of stars. Solid, dashed, and dash-dotted lines represent velocity differences in the x , y , and z directions. Blue lines show relative velocities between red and blue clumps, green lines are relative velocities between red and green clumps, and red lines indicate relative velocities between blue and green clumps,

(and future) simulation(s).²⁰ It would be useful to better characterize them, to understand how they form, and to have images of them. On the observational side, if the Λ CDM model and the Illustris simulation are reasonably accurate (and there is no evidence to suggest otherwise), it is of great interest to find such dark matter deficient galaxies (for example, more than 0.7% of SubhaloMassType $M_{\text{star}} \approx 2 \times 10^8 M_{\odot}$ galaxies should have SubhaloMassType $M_{\text{dm}}/M_{\text{star}} < 1$); they should provide an unusual and valuable perspective on cosmological structure formation and dark matter.

The dark matter deficient galaxy subhalo 476171 is much more massive and an outlier, but the Illustris simulation of the Λ CDM model results in many dark matter deficient ($M_{\text{dm}}/M_{\text{star}} < 1$) massive ($M_{\text{star}} > 10^{10} M_{\odot}$) galaxy subhalos. By studying the evolutionary history of subhalo 476171, we see that its progenitor massive subhalo contained a tightly bound cluster of stars. For some reason, perhaps as a consequence of gravitational interaction, this tightly-bound star cluster is kicked out of and escapes from its parent group. Perhaps because some of these stars are so tightly bound together, the massive subhalo 476171 and its stellar content largely preserve their structural integrity during the ejection process, losing only some stars but almost all dark matter, and so resulting in a dark matter deficient massive galaxy subhalo.

²⁰ Perhaps a detailed analysis of the Illustris raw particle data can provide more information about the dark matter deficient galaxy subhalos we have found, especially those subhalos which first appear at snap 135.

While it is clearly important to understand how the dark matter deficient massive galaxy subhalo 476171 (and its less extreme cousins) formed, if the Illustris simulation and the Λ CDM structure formation model are accurate then such objects should exist in the real universe (for example, more than 0.4% of galaxies with SubhaloMassType $M_{\text{star}} \approx 10^9 M_{\odot}$ should have SubhaloMassType $M_{\text{dm}}/M_{\text{star}} < 1$). Due to the large stellar mass of subhalo 476171, its r band magnitude is about -21 , bright enough for us to detect it. It is of great interest to search for such objects; perhaps these are the MUGs.

We are indebted to F. Marinacci, J. Peebles, V. Springel, and M. Vogelsberger for valuable advice, comments, and discussion. We acknowledge valuable discussions with P. Gagrani, C.-G. Park, L. Samushia, and L. Weaver. This work is supported by the National Basic Research Program of China (973 Program, grant No. 2014CB845800), the National Natural Science Foundation of China (grants 11422325, 11373022, and U1831207), the Excellent Youth Foundation of Jiangsu Province (BK20140016), and by DOE grant DE-SC0019038. H.Y. also acknowledges support by the China Scholarship Council for studying abroad.

REFERENCES

- Alam, S., Ata, M., Bailey, S., et al. 2017, MNRAS, 470, 2617 [arXiv:1607.03155]
- Blakeslee, J. P., & Cantiello, M. 2018, arXiv:1808.02176
- Buitrago, F., Ferreras, I., Kelvin, L. S., et al. 2018, arXiv:1807.02534
- Famaey, B., McGaugh, S., & Milgrom, M., 2018, arXiv:1804.04167
- Farooq, O., Crandall, S., & Ratra, B. 2013, Phys. Lett. B, 726, 72 [arXiv:1305.1957]
- Farooq, O., Madiyar, F. R., Crandall, S., & Ratra, B. 2017, ApJ, 835, 26 [arXiv:1607.03537]
- Farooq, O., & Ratra, B. 2013, ApJ, 766, L7 [arXiv:1301.5243]
- Fischler, W., Ratra, B., & Susskind, L. 1985, Nucl. Phys. B, 259, 730
- Genel, S., Vogelsberger, M., Springel, V., et al. 2014, MNRAS, 445, 175 [arXiv:1405.3749]
- Guth, A. H., & Pi, S.-Y. 1982, Phys. Rev. Lett., 49, 1110
- Haridasu, B. S., Luković, V. V., Moresco, M., & Vittorio, N. 2018, arXiv:1805.03595
- Hawking, S. W. 1982, Phys. Lett. B, 115, 295
- Hinshaw, G., Larson, D., Komatsu, E., et al. 2013, ApJS, 208, 19 [arXiv:1212.5226]
- Jesus, J. F., Holanda, R. F. L., & Pereira, S. H. 2018, JCAP, 1805, 073 [arXiv:1712.01075]
- Laporte, C. F. P., Agnello, A., & Navarro, J. F., 2018, arXiv:1804.04139
- Luković, V. V., Haridasu, B. S., & Vittorio, N. 2018, arXiv:1801.05765
- Martin, J. 2012, C. R. Physique, 13, 566 [arXiv:1205.3365]
- Martin, N. F., Collins, M. L. M., Longeard, N., & Tollerud, E. 2018, ApJ, in press [arXiv:1804.04136]
- Mitra, S., Choudhury, T. R., & Ratra, B. 2018, MNRAS, 479, 4566 [arXiv:1712.00018]
- Moresco, M., Pozzetti, L., Cimatti, A., et al. 2016, JCAP, 1605, 014 [arXiv:1601.01701]
- Nusser, A. 2018, arXiv:1806.01812
- Ooba, J., Ratra, B., & Sugiyama, N. 2018a, ApJ, 864, 80 [arXiv:1707.03452]
- Ooba, J., Ratra, B., & Sugiyama, N. 2017, arXiv:1710.03271
- Ooba, J., Ratra, B., & Sugiyama, N. 2018b, ApJ, in press [arXiv:1712.08617]
- Ooba, J., Ratra, B., & Sugiyama, N. 2018c, arXiv:1802.05571
- Park, C.-G., & Ratra, B. 2018a, arXiv:1801.00213
- Park, C.-G., & Ratra, B. 2018b, arXiv:1803.05522
- Park, C.-G., & Ratra, B. 2018c, arXiv:1807.07421
- Park, C.-G., & Ratra, B. 2018d, arXiv:1809.03598
- Peebles, P. J. E. 1982, ApJ, 263, L1
- Peebles, P. J. E. 1984, ApJ, 284, 439
- Planck Collaboration, Ade, P. A. R., Aghanim, N., Arnaud, M., et al. 2016, A&A, 594, A13 [arXiv:1502.01589]
- Ratra, B., & Vogeley, M. 2008, PASP, 120, 235 [arXiv:0706.1565]
- Ryan, J., Doshi, S., & Ratra, B. 2018, MNRAS, 480, 759 [arXiv:1805.06408]
- Scarpa, R., Hernandez, X., Martin, R. A. C., Falomo, R., & López-Corredoira, M. 2018, arXiv:1804.04817
- Scolnic, D. M., Jones, D. O., Rest, A., et al. 2017, arXiv:1710.00845
- Sijacki, D., Vogelsberger, M., Genel, S., et al. 2015, MNRAS, 452, 575 [arXiv:1408.6842]
- Starobinsky, A. A. 1982, Phys. Lett. B, 117, 175
- Trujillo, I., Beasley, M. A., Borlaff, A., et al. 2018, arXiv:1806.10141
- van Dokkum, P., Danieli, S., Cohen, Y., & Conroy, C. 2018c, ApJ, 864, L18 [arXiv:1807.06025]
- van Dokkum, P., Cohen, Y., Danieli, S., et al. 2018b, ApJ, 856, L30 [arXiv:1803.10240]

- van Dokkum, P., Danieli, S., Cohen, Y., et al. 2018a, *Nature*, 555, 629 [arXiv:1803.10237]
- Vogelsberger, M., Genel, S., Sijacki, D., et al. 2013, *MNRAS*, 436, 3031 [arXiv:1305.2913]
- Vogelsberger, M., Genel, S., Springel, V., et al. 2014a, *Nature*, 509, 177 [arXiv:1405.1418]
- Vogelsberger, M., Genel, S., Springel, V., et al. 2014b, *MNRAS*, 444, 1518 [arXiv:1405.2921]
- Wasserman, A., Romanowsky, A. J., Brodie, J., et al. 2018, arXiv:1807.07069
- Yu, H., Ratra, B., & Wang, F.-Y. 2018, *ApJ*, 856, 3 [arXiv:1711.03437]